

An Empirical Study of Quantum Dynamics as a Ground State Problem with Neural Quantum States

Vladimir Vargas-Calderón^{1†}, Herbert Vinck-Posada¹ and
Fabio A. González²

¹Grupo de Superconductividad y Nanotecnología, Departamento de Física
Universidad Nacional de Colombia, 111321, Bogotá, Colombia

²MindLab Research Group, Departamento de Ingeniería de Sistemas e Industrial
Universidad Nacional de Colombia, 111321, Bogotá, Colombia

E-mail: [†]vvargasc@unal.edu.co

Abstract. Neural quantum states are variational wave functions parameterised by artificial neural networks, a mathematical model studied for decades in the machine learning community. In the context of many-body physics, methods such as variational Monte Carlo with neural quantum states as variational wave functions are successful in approximating, with great accuracy, the ground-state of a quantum Hamiltonian. However, all the difficulties of proposing neural network architectures, along with exploring their expressivity and trainability, permeate their application as neural quantum states. In this paper, we consider the Feynman-Kitaev Hamiltonian for the transverse field Ising model, whose ground state encodes the time evolution of a spin chain at discrete time steps. We show how this ground state problem specifically challenges the neural quantum state trainability as the time steps increase because the true ground state becomes more entangled, and the probability distribution starts to spread across the Hilbert space. Our results indicate that the considered neural quantum states are capable of accurately approximating the true ground state of the system, i.e., they are expressive enough. However, extensive hyper-parameter tuning experiments point towards the empirical fact that it is poor trainability—in the variational Monte Carlo setup—that prevents a faithful approximation of the true ground state.

1. Introduction

A central problem of physics, be it fundamental quantum physics or applications for quantum technology, is the ground state problem. It can be defined as finding a state vector $|\Psi\rangle$ that minimises the expected value of the Hamiltonian \hat{H} that represents the energetic interactions between subsystems of a physical system. It is well-known that the difficulty of the ground state problem for a physical system arises from the exponential growth of the Hilbert space with respect to the number of the system components and their dimension. Therefore, techniques such as exact diagonalisation of \hat{H} quickly render insufficient to find the ground state, and other approximate methods have to be used.

In this work, we study the time evolution of the transverse field Ising model (TFIM) Hamiltonian in the context of the Feynman-Kitaev formalism [20], which appends a clock as an auxiliary subsystem of the main physical system, i.e. the Hilbert space \mathcal{H} of the whole system is $\mathcal{H} = \mathcal{P} \otimes \mathcal{C}$, where \mathcal{P} is the Hilbert space of the main physical system and \mathcal{C} is the Hilbert space of the clock. In this formalism, it is possible to build a Hamiltonian $\hat{\mathcal{H}}$ whose ground state $|\Psi\rangle \propto \sum_t |\psi(t)\rangle \otimes |t\rangle$ encodes the time evolution history of the main physical system, where $|\psi(t)\rangle$ its state at time t , and $|t\rangle$ is the state of the clock signalling time t [22]. This means that the combined state can be projected onto one of the clock's states that represents a specific time to get the state of the physical system at that particular time, i.e. $|\psi(t)\rangle \propto \langle\Psi|t\rangle$.

Recently, Barison et al. [6] mapped the Hamiltonian $\hat{\mathcal{H}}$ to a qubit Hamiltonian $\hat{\mathcal{H}}_Q$ with the same spectrum, and they find its ground state using the variational quantum eigensolver [19] (VQE) method with a parameterised quantum circuit. VQE consists of using a quantum computer to build a circuit composed of rotation gates whose angles are parameters that can be optimised. Such a circuit might be written as $V(\boldsymbol{\vartheta})$, where $\boldsymbol{\vartheta}$ are the gate parameters. Then, the circuit prepares the normalised quantum state $|\phi_{\boldsymbol{\vartheta}}\rangle = V(\boldsymbol{\vartheta})|0, \dots, 0\rangle$, where the state $|0, \dots, 0\rangle$ is the trivial all-zeros state that is normally used when initialising a quantum circuit. After preparing the quantum state, it is used to measure the exact variational energy $E_{\boldsymbol{\vartheta}} = \langle\phi_{\boldsymbol{\vartheta}}|\hat{\mathcal{H}}_Q|\phi_{\boldsymbol{\vartheta}}\rangle$, and also to measure its derivatives with respect to each variational parameter. Then, a classical computer is used to update the parameters, given an optimisation routine such as stochastic gradient descent. However, we emphasise that the quantum circuit of VQE is simulated on a classical computer, which enables the exact access to the variational state $|\phi_{\boldsymbol{\vartheta}}\rangle$. Therefore, the variational energy $E_{\boldsymbol{\vartheta}}$ is not estimated, as it would be on a real quantum device, but can be computed exactly. The same occurs with the gradients of the variational energy with respect to variational parameters. On a real quantum device, however, these quantities have to be estimated, which is both time-consuming and introduces inaccuracy. Moreover, scalability of VQE to study large spin chains might be endangered by trainability issues in variational quantum circuits [4] such as the onset of barren plateaus [23].

The aforementioned limitations of VQE motivate us to approach the Feynman-Kitaev Hamiltonian through one of the most successful methods to solve the ground state problem: variational Monte Carlo (VMC) [8], which aims to solve the problem $\min_{\boldsymbol{\theta}} \langle\Psi_{\boldsymbol{\theta}}|\hat{H}|\Psi_{\boldsymbol{\theta}}\rangle / \langle\Psi_{\boldsymbol{\theta}}|\Psi_{\boldsymbol{\theta}}\rangle$ (for any Hamiltonian \hat{H}), where $|\Psi_{\boldsymbol{\theta}}\rangle$ is a variational wave function, parameterised by some parameters $\boldsymbol{\theta}$. VMC stands out because it takes advantage of the usual sparsity of the Hamiltonian, and the fact that the ground state usually lies in a so-called “small corner” of the Hilbert space, meaning that only a small subset of elements of the Hilbert space basis is needed to accurately characterise the ground state (see more details about VMC in section 3).

Recently, it has been shown that an outstanding parameterisation of variational wave functions can be achieved by bringing tools from the machine learning community; in particular, wave functions can be parameterised by artificial neural networks, giving

birth to the so-called neural quantum states (NQSs)[‡] [11]. Unfortunately, this means that the open questions from artificial neural networks also permeate their application to quantum physics. In particular, there are two main areas of concern: expressivity and trainability. Expressivity refers to the capacity that a parameterisation has to reproduce arbitrary wave functions [24, 16, 25]. More precisely, a parameterised wave function defines a subset of all the possible wave functions; the larger this subset is, the more expressive the parameterisation is [26, 28]. On the other hand, trainability refers to the capacity that an algorithm has to update the parameters so that a cost function—the expected value of \hat{H} —is minimised, taking into account the intricacy of said cost function [36].

Limitations in expressivity and trainability in machine learning models used as NQSs also limit the possibility to successfully find ground states of Hamiltonians. Therefore, it is imperative to understand what features found in a Hamiltonian can expose such limitations.

We provide a systematic study of trainability and show that training NQSs through VMC to find the ground state of the Hamiltonian \mathcal{H} is particularly difficult because the clock’s degrees of freedom entangle with the main physical system, making the ground state $|\Psi\rangle$ not only highly entangled, but also in need of a large portion of the canonical basis of the Hilbert space \mathcal{H} to be described.

This paper is divided as follows. In section 2 we introduce the Feynman-Kitaev formalism. In section 3 we present the NQSs used in our work and explain how VMC works. Then, we present the results, which include an extensive study of VMC and NQSs hyper-parameters, in section 4. We discuss our empirical findings in section 5. Finally, we conclude in section 6.

2. The Feynman-Kitaev formalism

Suppose that we want to evolve the quantum state of a physical system $|\psi(t_0)\rangle \in \mathcal{P}$ to a later time T . The formal solution of this problem is given by the Schrödinger equation, which asserts that $|\psi(T)\rangle = \hat{U}(T, t_0) |\psi(t_0)\rangle$, where U is the time evolution operator that takes the form (we consider $\hbar = 1$) $\hat{\mathcal{T}} \exp\left(-i \int_{t_0}^T \hat{H}(t') dt'\right)$, with $\hat{\mathcal{T}}$ being the time ordering operator. If the Hamiltonian is time independent, it is possible to write the time evolution operator simply as $\hat{U}(T, t_0) = \hat{U}(T - t_0) = \exp\left(-i \hat{H}(T - t_0)\right)$. To avoid verbosity, we set $t_0 = 0$ throughout the paper. It is worth highlighting that, even though \hat{H} is usually sparse, $\hat{U}(T)$ need not be sparse, especially for large values of T [3]. Therefore, computing the matrix representation of $\hat{U}(T)$ involves a considerable computational effort. It is much easier to compute $\hat{U}(\Delta t)$ for $\Delta t = T/N \ll T$ for large N , as $\hat{U}(\Delta t)$ becomes just a perturbation of the identity. Nonetheless, if one has easy computational access to $\hat{U}(\Delta t)$ but not to $\hat{U}(T)$, in order to evolve the system to a

[‡] Many of the different methods associated to NQSs have even been standardised in open-source libraries such as NetKet [31], which facilitates the use of these tools for researchers. All of the experiments of this paper involving VMC were done using NetKet.

time T one has to evolve the system in N steps of size Δt , which ends up matching the computational effort of directly computing $\hat{U}(T)$.

One of the earliest proposals for performing a quantum computation was precisely that of the time evolution of a quantum system [13]. The idea behind this proposal is that the quantum state of a physical system can be described along with the quantum state of a clock [22]. In particular, the clock can be in the states $|0\rangle, |1\rangle, \dots, |N\rangle \in \mathcal{C}$, i.e., it is a $N+1$ -level system in the Hilbert space \mathcal{C} . We encode the $N+1$ -level system that describes the clock in $N_T = \lceil \log_2(N+1) \rceil$ spins. As Barison et al. [6], we also consider the reflected binary code to map a state $|t\rangle$ to the state of N_T spins because two consecutive states $|t\rangle$ and $|t+1\rangle$ are mapped to states of N_T spins where only one spin is different. Thus, the physical spin chain is enlarged with spins representing the state of the clock, as shown in fig. 1(a).

McClean et al. [22] showed that a variational principle can help in constructing a Hamiltonian $\hat{\mathcal{H}}$ of the whole system such that its ground state is precisely

$$|\Psi\rangle = \frac{1}{\sqrt{N+1}} \sum_{t=0}^N |\psi(t)\rangle \otimes |t\rangle. \quad (1)$$

The Hamiltonian of the whole system can be written as [22, 10, 6]

$$\hat{\mathcal{H}} = \hat{\mathcal{H}}_0 + \frac{1}{2} \sum_{t=0}^{N-1} \left[I_{\mathcal{P}} \otimes (|t\rangle\langle t| + |t+1\rangle\langle t+1|) + \{\hat{U}(\Delta t) \otimes |t+1\rangle\langle t| + \text{h.c.}\} \right], \quad (2)$$

where $I_{\mathcal{P}}$ is the identity of the physical system's Hilbert space \mathcal{P} and $\hat{\mathcal{H}}_0 = \hat{H}_0 \otimes |0\rangle\langle 0|$ is a term that breaks the degeneracy of the ground state by fixing the initial state at $t = 0$. For instance, Barison et al. [6] take $\hat{H}_0 = I - |\psi(0)\rangle\langle\psi(0)|$, for any desired initial state of the physical system $|\psi(0)\rangle$. Remarkably, the ground state of eq. (2) is exactly eq. (1), and its energy is $\langle\Psi|\hat{\mathcal{H}}|\Psi\rangle = 0$. This property is important because it allows us to quantify how close the algorithm is to converge to the true ground state of the system.

In this work, we study the dynamics of the prototypical TFIM Hamiltonian defined on a one-dimensional chain of N_S (ordered) spins:

$$\hat{H} = J \sum_{i=1}^{N_S-1} \hat{\sigma}_i^z \hat{\sigma}_{i+1}^z + h \sum_{i=1}^{N_S} \hat{\sigma}_i^x, \quad (3)$$

where $\hat{\sigma}_i^{z(x)}$ is the Z(X) Pauli operator acting only on spin i . Throughout the paper, we use $J = 0.25$ and $h = 1$.

3. Variational Monte Carlo and neural quantum states

The variational Monte Carlo (VMC) method leverages the variational method of quantum mechanics to problems with intractable Hilbert spaces [8]. The

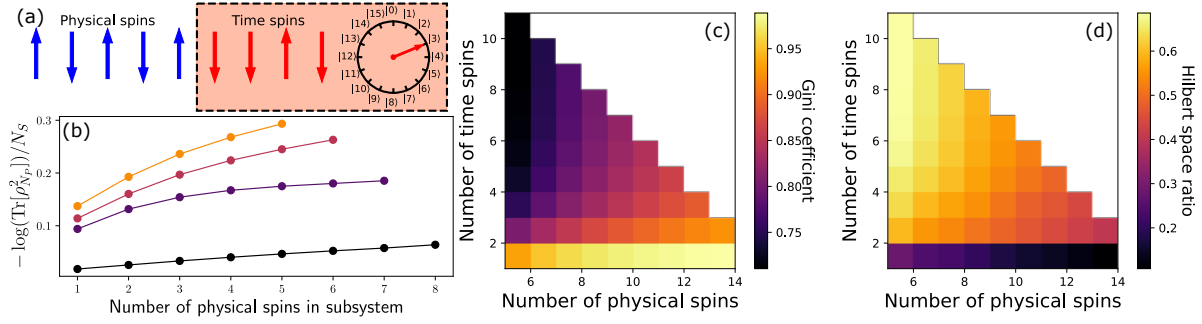


Figure 1. Representation of the physical spin chain enlargement with a clock state (a); and properties of the ground state of the enlarged Hamiltonian in eq. (2) found with exact diagonalisation. (b) shows the second Rényi entropy per spin of a sub-chain of physical spins. (c) shows the Gini coefficient of the probability distribution of the ground state, and (d) shows the ratio of the canonical basis of the Hilbert space that is needed to explain 99% of the probability of the ground state. The main text (section 4) explains these plots in-depth.

variational method proposes a parameterised ansatz $|\Psi_\theta\rangle$ and poses the problem $\min_\theta \langle \Psi_\theta | \hat{\mathcal{H}} | \Psi_\theta \rangle / \langle \Psi_\theta | \Psi_\theta \rangle$, where the energy is minimised, under the principle that it is only the ground state that has the minimum energy possible. The problem is often difficult due to the non-convexity of the function to be minimised. However, it is the dimensionality of the problem that renders it prohibitive to solve. Indeed, by considering the completeness relation $I_{\mathcal{H}} = \sum_\sigma |\sigma\rangle\langle\sigma|$ of a Hilbert space \mathcal{H} with an orthonormal basis $\{|\sigma\rangle\}$ ($|\sigma\rangle$ is a spin configuration—in the case of the TFIM expanded with a clock—of the explicit form $|\sigma\rangle = |\sigma_1\rangle \otimes |\sigma_2\rangle \otimes \cdots \otimes |\sigma_{N_S+N_T}\rangle \equiv |\sigma_1, \dots, \sigma_{N_S+N_T}\rangle$ with $|\sigma_i\rangle \in \{|\uparrow\rangle, |\downarrow\rangle\}$), we have that the variational energy is

$$E_\theta = \frac{\langle \Psi_\theta | I_{\mathcal{H}} \hat{\mathcal{H}} I_{\mathcal{H}} | \Psi_\theta \rangle}{\langle \Psi_\theta | I_{\mathcal{H}} I_{\mathcal{H}} | \Psi_\theta \rangle} = \sum_{\sigma, \sigma'} P_\theta(\sigma) \langle \sigma | \hat{\mathcal{H}} | \sigma' \rangle \frac{\Psi_\theta(\sigma')}{\Psi_\theta(\sigma)}, \quad (4)$$

where $P_\theta(\sigma) = |\Psi_\theta(\sigma)|^2 / \sum_{\sigma'} |\Psi_\theta(\sigma')|^2$ is the probability of the configuration σ . The usual minimisation of E_θ with respect to the parameters of the wave function can be performed using any optimisation algorithm. However, as mentioned, it is practically impossible to perform the double summation because of the size of the Hilbert space \mathcal{H} . Instead, VMC estimates E_θ by virtue of the empirical fact that the ground state is usually on a “small corner” of the Hilbert space, meaning that $P_\theta(\sigma) \approx 0$ for almost every σ , except for a small subset of the basis. Therefore, the estimation of the variational energy is simply [8, 11]

$$E_\theta^* = \left\langle \sum_{\sigma'} \langle \sigma | \hat{\mathcal{H}} | \sigma' \rangle \frac{\Psi_\theta(\sigma')}{\Psi_\theta(\sigma)} \right\rangle_{\sigma \in \mathcal{M}}, \quad (5)$$

where the average is taken only using configurations from a sample \mathcal{M} that is built according to the distribution $P_\theta(\sigma)$. Remarkably, since $\hat{\mathcal{H}}$ is usually sparse in the canonical basis $\{|\sigma\rangle\}$, the matrix elements $\langle \sigma | \hat{\mathcal{H}} | \sigma' \rangle$ are zero for most configurations σ'

given a fixed σ . Another important feature of eq. (5) is that the wave function need not be normalised to estimate the energy, or any other observable. We also emphasise that, in the case of the Feynman-Kitaev Hamiltonian (eq. (2)) estimations of observables have to be multiplied by $N + 1$ to account for the normalisation factor of the history state in eq. (1).

Carleo and Troyer [11] introduced the idea of using neural networks to represent the wave function, i.e., the parameters θ are the parameters of a neural network that takes as input a configuration σ and outputs a complex number $\Psi_\theta(\sigma)$. These models receive the name of neural quantum states (NQSS). A common choice of neural network is the restricted Boltzmann machine (RBM) [11], which induces the ansatz:

$$\Psi_\theta^{\text{RBM}}(\sigma) = \exp\left(\sum_{j=1}^{N_S+N_T} a_j \sigma_j\right) \prod_{\ell=1}^{N_H} 2 \cosh\left(b_\ell + \sum_{j=1}^{N_S+N_T} W_{\ell,j} \sigma_j\right), \quad (6)$$

where N_H is the number of hidden units of the RBM and $\{a_j, b_j, W_{\ell,j}\}$ is the set of complex parameters. The total number of parameters of this ansatz is $N_H(N_S + N_T + 1)$.

The sample \mathcal{M} is built, in the case of the RBM, with the Metropolis-Hastings algorithm [17] because it is able to sample from a non-normalised distribution, such as the one induced by eq. (6). Indeed, normalising the RBM ansatz is computationally intractable for long spin chains. The Metropolis-Hastings algorithm chosen in this study comprises the following steps: (i) A random configuration $\sigma^{(0)}$ is generated. (ii) At iteration $r \geq 1$ we take the configuration $\sigma^{(r-1)}$ and randomly flip one spin, forming a candidate configuration $\tilde{\sigma}^{(r)}$. (iii) $\sigma^{(r)}$ is set to $\tilde{\sigma}^{(r)}$ with probability $|\Psi_\theta^{\text{RBM}}(\tilde{\sigma}^{(r)})|^2 / |\Psi_\theta^{\text{RBM}}(\sigma^{(r-1)})|^2$, else it is set to $\sigma^{(r-1)}$. Usually, these steps are repeated until thermalisation, which means that the Markov chain stabilises, and only then one starts to collect configurations to build the sample \mathcal{M} .

However, stabilising Markov chains can be difficult, and in some cases might require a prohibitive amount of sampling in order to get a good representation of the probability distribution that needs to be approximated [32]. For this reason, we also consider autoregressive models whose probability distribution can be sampled exactly, meaning that the sample \mathcal{M} can be gathered by directly accessing the probability distribution $P_\theta(\sigma)$. In particular, we adopt a chain-type Bayesian network [14, 34, 35, 37] as the building block of the autoregressive model, which defines $P_\theta(\sigma) = q_\theta(\sigma_1) \prod_{i=2}^{N_S+N_T} q_\theta(\sigma_i | \sigma_1, \dots, \sigma_{i-1})$. Here, q_θ models the probability that the i -th spin has a specified value conditioned on the observed values for the previous spins. These conditional probabilities are connected to the quantum mechanical state vector through the Born rule, i.e. $q_\theta(\sigma_i | \sigma_1, \dots, \sigma_{i-1}) \equiv |\Psi_\theta^{\text{AR}}(\sigma_i | \sigma_1, \dots, \sigma_{i-1})|^2$. The form of the actual wave function is a two-component conditional amplitude vector $\eta(\sigma_i | 1, \dots, \sigma_{i-1}) = (\eta_1^i, \eta_2^i)^T$, where η is an autoregressive neural network with two complex outputs per spin such that $|\eta_1^i|^2 + |\eta_2^i|^2 = 1$. Therefore, the actual amplitude of a spin configuration can be simply found by considering the vector representation of the possible values for a spin, which we denote as σ_i , that can be either $(1, 0)^T$ for $\sigma_i = +1$ or $(0, 1)^T$ for

$\sigma_i = -1$. Thus, we write the amplitude of a spin configuration given by the model as

$$\Psi_{\theta}^{\text{AR}}(\sigma) = \prod_{i=1}^{N_S+N_T} \sigma_i \cdot \eta(\sigma_i | 1, \dots, \sigma_{i-1}). \quad (7)$$

4. Results

We find the ground state of eq. (2), which encodes the time evolution of a system governed by the TFIM Hamiltonian in eq. (3). The initial state is set as $|\uparrow, \dots, \uparrow\rangle$, achieved by setting $\hat{H}_0 = \frac{1}{2} \sum_{i=1}^{N_S} (1 - \hat{\sigma}_i^z)$. There is an intrinsic difficulty in the Feynman-Kitaev Hamiltonian, which is that a lot of information (the quantum state of the Ising chain at each time step) needs to be stored in the ground state. Such difficulty is evident from analysing the structure of the ground state. First, we consider a system where the total number of spins is $N_T + N_S = 9$, which fixes the Hilbert space size to $|\mathcal{H}| = 2^9$. We assign N_S spins to the physical TFIM, and N_T spins to encode 2^{N_T} time steps, from zero to a time $T = 3$. Let $|\Phi(N_T)\rangle$ be the ground state found through exact diagonalisation of eq. (2). We can quantify the entanglement scale of the system by measuring the second Rényi entropy per physical spin $-\log(\text{Tr}[\rho_{N_P}^2])/N_S$ [29]. Here, ρ_P is the reduced density matrix, which is obtained by tracing over all the spin degrees of freedom except the first $N_P \leq N_S$ physical spins from the ground state, i.e, $\rho_{N_P} = \sum_{\sigma_{N_P+1}, \dots, \sigma_{N_S+N_T}} \langle \sigma_{N_P+1}, \dots, \sigma_{N_S+N_T} | \Phi(N_T) \rangle \langle \Phi(N_T) | \sigma_{N_P+1}, \dots, \sigma_{N_S+N_T} \rangle$. Figure 1(b) shows the second Rényi entropy per physical spin, showing that the entanglement increases between the first N_P physical spins and the rest of the system as more spins are dedicated to encode time steps. Indeed, the last point of each curve in fig. 1(b) show that the entanglement between the time spins and the physical spins increase as long as more spins are used to encode the quantum state of the clock.

Another insightful analysis that summarises the complexity of the ground state of eq. (2) is the Gini coefficient of the probability distribution [15]. The Gini coefficient is normally used in the context of economics to assess the concentration of wealth in a society: the highest the concentration of wealth in a few individuals, the higher the Gini coefficient will be; on the other hand, it will tend to zero if wealth is perfectly distributed among the population. If we think of probability as wealth and of elements of the canonical basis as individuals, the analogy is clear. Therefore, we measure the Gini coefficient as

$$G = \frac{\sum_{\sigma, \sigma'} ||\langle \sigma | \Phi(N_S) \rangle|^2 - |\langle \sigma' | \Phi(N_S) \rangle|^2|}{2|\mathcal{H}| \sum_{\sigma} |\langle \sigma | \Phi(N_S) \rangle|^2}. \quad (8)$$

We show in fig. 1(c) the Gini coefficient for different values of physical spins N_S and time spins N_T . The most relevant reading of this plot for our work is considering the diagonals of the plot where $N_S + N_T$ is fixed. In such a case, we see that the larger N_T is, the smaller the Gini index is. This indicates that the probability spreads across more elements of the canonical basis of \mathcal{H} as N_T increases. Said fact is corroborated

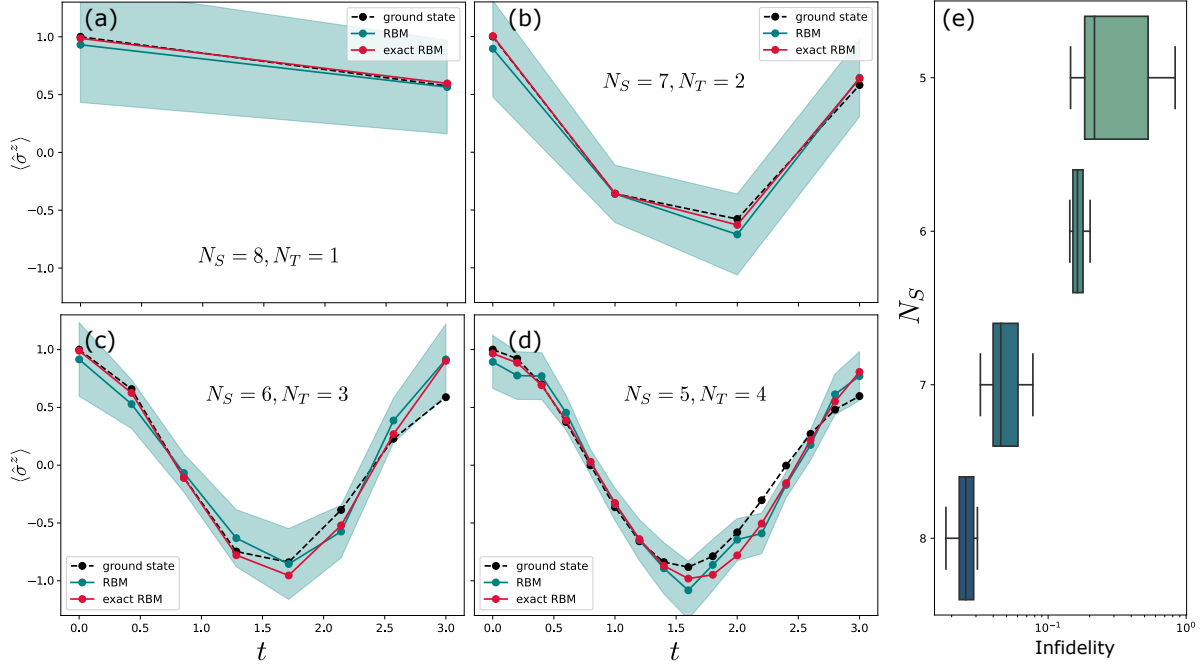


Figure 2. Time evolution approximated with an RBM as an NQS. (a)-(d) show the expected value of the average magnetisation $\langle \hat{\sigma}^z \rangle = \frac{1}{N_S} \sum_{i=1}^{N_S} \langle \hat{\sigma}_i^z \rangle$. In each panel curves are shown for the average magnetisation obtained through exact diagonalisation (ground state), estimation of the variational magnetisation with a sample \mathcal{M} (RBM) and exact variational magnetisation (exact RBM). The shaded region indicates the estimated fluctuations of magnetisation using the sample \mathcal{M} . The lines serve as guide for the eye only. (e) shows a box plot of infidelity $(1 - |\langle \Phi(N_S) | \Psi_{\theta^*}^{\text{RBM}} \rangle|^2)$ for the best 10 hyper-parameter experiments, where θ^* indicates that parameters have been optimised until convergence.

by fig. 1(d), which shows the ratio of the canonical basis elements needed to capture 99% of the probability distribution given by the ground state. More formally stated, let the canonical basis $\{\sigma\}$ be indexed such that $|\langle \sigma^{(i)} | \Phi(N_S) \rangle|^2 \geq |\langle \sigma^{(i+1)} | \Phi(N_S) \rangle|^2$. Then, fig. 1(d) shows the ratio $r/2^{N_S+N_T}$, where r is the smallest integer such that $\sum_{i=1}^r |\langle \sigma^{(i)} | \Phi(N_S) \rangle|^2 < 0.99$. It is clear from fig. 1(d) that for a fixed number of total spins $N_S + N_T$, the larger N_T is, the highest the ratio of elements in the canonical basis needed to explain the ground state is.

Figure 1 showed that the ground state, for large values of N_T , is not anymore in a “small corner” of the Hilbert space. Instead, a well-spread and highly entangled ground state forms. Figure 2 reflects this fact on the increasing difficulty of training an RBM as an NQS for the ground state through VMC as N_T grows. We fixed the total number of spins $N_S + N_T = 9$, as in fig. 1(b). For each value of N_T (between 1 and 4), we performed hyper-parameter tuning for 100 iterations with Optuna [2], aiming to minimise the variational energy in eq. (5). Details of the optimisation and hyper-parameter tuning can be found in Appendix A. Figure 2(a)-(d) show the time evolution of the spin chain for the hyper-parameters that produced the smallest infidelities.

It is seen in fig. 2(a)-(d) that, overall, the evolution of the average magnetisation is

in accordance to the average magnetisation obtained through exact diagonalisation for all the values of N_T . However, the qualitative agreement of magnetisation curves does not exhibit the difficulty of training the RBM as N_T increases. Indeed, the infidelities for fig. 2(a)-(d) are 0.018, 0.032, 0.144 and 0.145, respectively. The increasing infidelity, as N_T grows, indicates that training becomes more difficult, despite the Hilbert space always having the same size. However, these are only the best states found after hyper-parameter tuning. Figure 2(e) shows a box plot of the infidelities of the best 10 hyper-parameter tuning states, where a clear trend appears: the larger N_T is, the more difficult it is to find the correct ground state.

Regarding the autoregressive ansatz in eq. (7), we see in fig. 3 qualitatively similar, but worse performance in terms of correctly describing the evolution of magnetisation. This is further confirmed by poor infidelities when N_T is large. The lowest infidelities achieved after hyper-parameter tuning were 0.025, 0.063, 0.517 and 0.850 for fig. 3(a)-(d), respectively. Even though one can sample directly from the probability distribution induced by the autoregressive ansatz, avoiding issues with the Markov chain sampling, it is clear that capturing the ground state of eq. (2) is more challenging.

From fig. 3 stands out the fact that, in some cases, the average magnetisation exceeds the upper bound limit for the average magnetisation, which is one. This can be understood from the construction of the Feynman-Kitaev history state eq. (1). Explicitly, an observable \hat{O} at time t is measured as

$$O_{\theta}^* = (N + 1) \left\langle \sum_{\sigma'} \langle \sigma | (\hat{O} \otimes |t\rangle\langle t|) | \sigma' \rangle \frac{\Psi_{\theta}(\sigma')}{\Psi_{\theta}(\sigma)} \right\rangle_{\sigma \in \mathcal{M}}. \quad (9)$$

Therefore, it is possible that the probability associated to a particular time of the clock is greater than $1/(N + 1)$, making it possible to measure average magnetisations greater than one.

5. Discussion

In this section, we discuss the results so far presented in light of the recent study by Barison et al. [6]. Compared to VQE, as we saw in the previous section, VMC struggles with finding an accurate approximation of the true ground state, presenting infidelities at least one order of magnitude higher than infidelities reported by Barison et al. [6]. Unlike VMC, VQE directly handles a normalised quantum state in the whole Hilbert space, and its parameterisation consists of local transformations that preserve the norm. A natural set of questions that arise are: what is it that makes NQSs have larger infidelities than VQE? Is it expressivity? Is it trainability? [33, 1] If the NQS can represent the ground state of eq. (2) with low infidelity, it means that the NQS is expressive enough, but trainability hampers the possibility of describing the correct ground state, as shown in fig. 2.

Considering the previous discussion, let us explore the expressivity of the RBM NQS. The most challenging experiment tackled in this paper is the one of $N_S = 5$ and

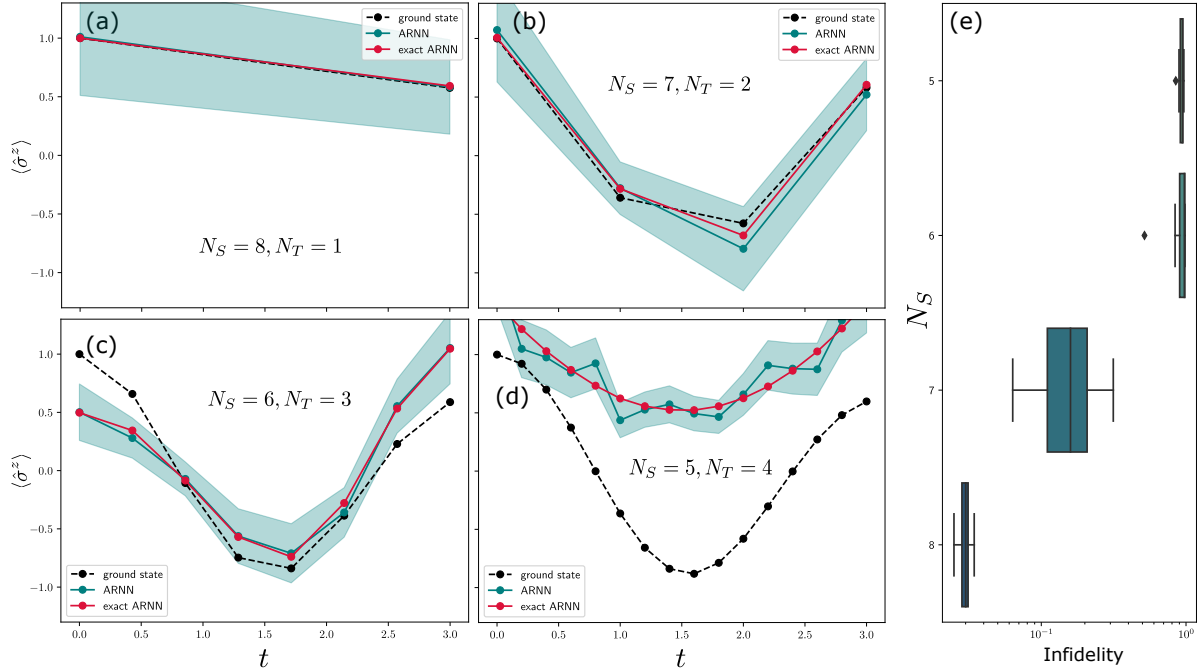


Figure 3. Similar to fig. 2 but for the autoregressive ansatz in eq. (7).

$N_T = 4$, which is perfectly tractable for a classical computer. We consider the problem of finding parameters for the RBM ansatz that are able to faithfully describe the ground state of eq. (2) by giving the RBM the ability to access the whole Hilbert space. To this end, we directly minimise the infidelity $1 - |\langle \Phi(N_S = 5) | \Psi_{\theta}^{\text{RBM}} \rangle|^2$. Experimentation with the ansatz in eq. (6) shows that training leads to local minima of the infidelity landscape, hinting convergence to stable excited states of eq. (2). Therefore, we turned over to a similar RBM ansatz, which defines an RBM for the modulus and another for the phase of the wave function [29]

$$\Psi_{\theta}^{\text{MP-RBM}} = \exp(\Psi_{\theta_{\text{Re}}}^{\text{RBM}} + i\Psi_{\theta_{\text{Im}}}^{\text{RBM}}), \quad (10)$$

where $\Psi_{\theta_{\text{Re}}}^{\text{RBM}}$ and $\Psi_{\theta_{\text{Im}}}^{\text{RBM}}$ are RBMs defined by eq. (6), with real-only parameters θ_{Re} and θ_{Im} . Training the MP-RBM ansatz in eq. (10) to minimise the estimated variational energy (see eq. (5)) with VMC yields similar infidelities than the RBM ansatz after hyper-parameter tuning (0.160 for the $N_S = 5, N_T = 4$ case). However, it is easier to train the MP-RBM when minimising the infidelity (even without hyper-parameter tuning). In fact, we see that the MP-RBM is capable of learning the ground state with an infidelity of 2×10^{-3} , as depicted by the excellent agreement between the MP-RBM magnetisation curve and the exact one in fig. 4.

Figure 4 exhibits the probability distribution of each state induced onto the canonical basis of the Hilbert space \mathcal{H} . Since the infidelity-optimised MP-RBM leads to a very low infidelity, differences between its distribution (top middle panel) and the exact ground state distribution (top left panel) are minimal. However, differences with the MP-RBM obtained through VMC are larger. This is reflected onto the average

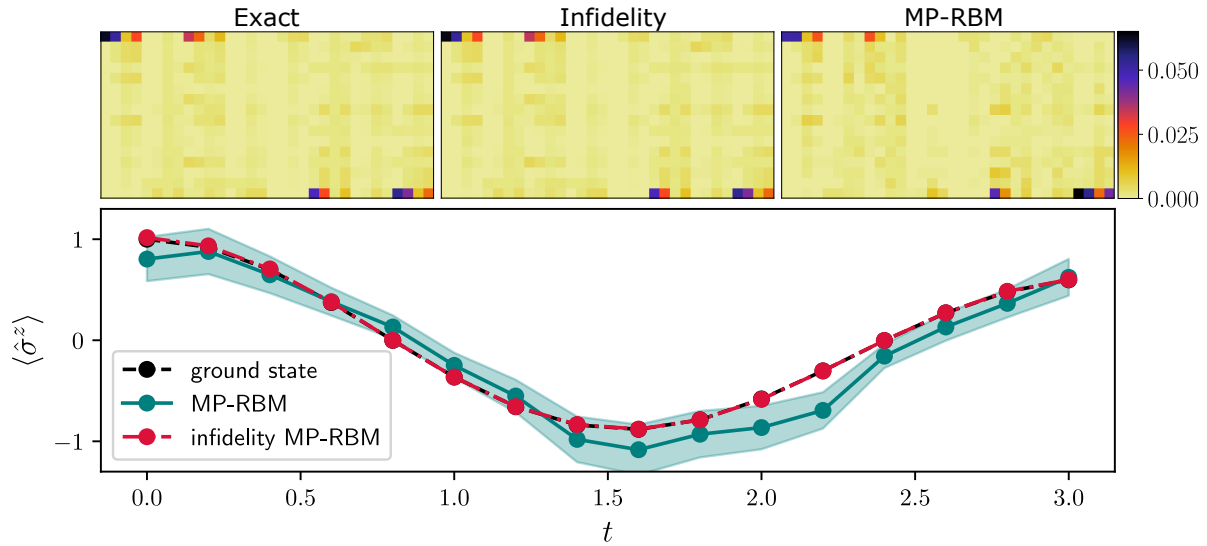


Figure 4. Probability of each element of the canonical basis of \mathcal{H} and time evolution of magnetisation for an MP-RBM ansatz. The top panel shows the 2^9 probabilities associated to each element of the canonical basis of \mathcal{H} for the ground states obtained through exact diagonalisation, through variational minimisation of the infidelity, and through variational minimisation of the estimated energy in the left, middle and right sub-panels, respectively. The bottom panel shows the average magnetisation obtained with each of these states.

magnetisation curves, shown in the bottom panel of fig. 4. These results are in agreement with the study by Deng et al. [12], who show that NQSs based on RBMs have a wide expressivity, able to represent many highly entangled quantum states.

Similar results are obtained for the autoregressive model. Again, we find that optimising the infidelity for the ansatz in eq. (7) traps the NQS into an excited state of eq. (2), which is why we turned over to an autoregressive ansatz that explicitly divides the modulus and phase of the wave function, similar to the works by Hibat-Allah et al. [18] and Barrett et al. [7]. In this setup, we divide the autoregressive neural network $\boldsymbol{\eta}$ into two autoregressive neural networks, one for the modulus, and the other for the phase of the wave function. Training this ansatz to minimise the estimated variational energy with VMC, yields high infidelity of 0.920 after hyper-parameter tuning for the $N_S = 5, N_T = 4$ case, which is a similar infidelity to the one obtained by the ansatz in eq. (7). On the other hand, the infidelity optimisation (without any hyper-parameter tuning) yields an infidelity of 3.5×10^{-3} , comparable to that of the MP-RBM. This result further supports the fact that NQSs are able to accurately approximate highly entangled ground states with widely-spread probability distributions. The problem, however, resides on trainability when performing VMC. An important final remark is that knowing the reason why infidelity optimisation consistently fails for NQSs with complex-only parameters remains an open question.

6. Conclusions

We studied the time-evolution of a transverse field Ising model through the Feynman-Kitaev Hamiltonian, which encodes the state of a physical system at a given set of equidistant time instances into the state of an enlarged quantum mechanical system (it is enlarged by the state of a clock). The ground state of the Feynman-Kitaev Hamiltonian was systematically searched by tuning hyper-parameters of neural quantum state ansätze through the variational Monte Carlo method.

We showed that neural quantum states encounter difficulty in representing a highly-entangled ground state whose probability distribution is well-spread across the canonical basis of the Hilbert space. As the number of clock states increased, we consistently saw that the performance of neural quantum states deteriorated, yielding lower fidelities to the true ground state of the Feynman-Kitaev Hamiltonian. The characterisation of such ground state showed that as the number of clock states increased, both entanglement quantifiers and probability spread also increased. These features explain that the ground state is ever more complicated for the neural quantum state to learn through variational Monte Carlo.

However, we also saw that the degrading performance of neural quantum states was not because of a lack of expressivity of the neural quantum state per se, as also supported by previous literature. Instead, we provide evidence that trainability—in the variational Monte Carlo setup—is the main source of under-performance, even for autoregressive models, which sample directly from the probability distribution induced by the variational state. This supports the hypothesis that optimisation techniques, and not sampling, degrade the quality of the ground state, accompanied by the fact that energy convergence does not ensure convergence of the state (at least not in the same time scale) [30, 5].

References

- [1] A. Abbas, D. Sutter, C. Zoufal, A. Lucchi, A. Figalli, and S. Woerner. The power of quantum neural networks. *Nature Computational Science*, 1(6):403–409, 2021. doi: 10.1038/s43588-021-00084-1. URL <https://doi.org/10.1038/s43588-021-00084-1>.
- [2] T. Akiba, S. Sano, T. Yanase, T. Ohta, and M. Koyama. Optuna: A next-generation hyperparameter optimization framework. In *Proceedings of the 25rd ACM SIGKDD International Conference on Knowledge Discovery and Data Mining*, 2019.
- [3] Á. M. Alhambra. Quantum many-body systems in thermal equilibrium, 2022. URL <https://arxiv.org/abs/2204.08349>.
- [4] E. R. Anschuetz and B. T. Kiani. Beyond barren plateaus: Quantum variational algorithms are swamped with traps, 2022. URL <https://arxiv.org/abs/2205.05786>.

- [5] L. E. Ballentine. *Quantum mechanics: a modern development*. World Scientific Publishing Company, 2014.
- [6] S. Barison, F. Vicentini, I. Cirac, and G. Carleo. Variational dynamics as a ground-state problem on a quantum computer. *arXiv preprint arXiv:2204.03454*, 2022.
- [7] T. D. Barrett, A. Malyshev, and A. I. Lvovsky. Autoregressive neural-network wavefunctions for ab initio quantum chemistry. *Nature Machine Intelligence*, 4(4):351–358, 2022. doi: 10.1038/s42256-022-00461-z. URL <https://doi.org/10.1038/s42256-022-00461-z>.
- [8] F. Becca and S. Sorella. *Quantum Monte Carlo approaches for correlated systems*. Cambridge University Press, 2017.
- [9] J. Bergstra, R. Bardenet, Y. Bengio, and B. Kégl. Algorithms for hyperparameter optimization. In J. Shawe-Taylor, R. Zemel, P. Bartlett, F. Pereira, and K. Weinberger, editors, *Advances in Neural Information Processing Systems*, volume 24. Curran Associates, Inc., 2011. URL <https://proceedings.neurips.cc/paper/2011/file/86e8f7ab32cfd12577bc2619bc635690-Paper.pdf>.
- [10] L. Caha, Z. Landau, and D. Nagaj. Clocks in feynman’s computer and kitaev’s local hamiltonian: Bias, gaps, idling, and pulse tuning. *Phys. Rev. A*, 97:062306, Jun 2018. doi: 10.1103/PhysRevA.97.062306. URL <https://link.aps.org/doi/10.1103/PhysRevA.97.062306>.
- [11] G. Carleo and M. Troyer. Solving the quantum many-body problem with artificial neural networks. *Science*, 355(6325):602–606, 2017.
- [12] D.-L. Deng, X. Li, and S. Das Sarma. Quantum entanglement in neural network states. *Phys. Rev. X*, 7:021021, May 2017. doi: 10.1103/PhysRevX.7.021021. URL <https://link.aps.org/doi/10.1103/PhysRevX.7.021021>.
- [13] R. P. Feynman. Quantum mechanical computers. *Optics News*, 11(2):11–20, Feb 1985. doi: 10.1364/ON.11.2.000011. URL <http://www.optica-opn.org/abstract.cfm?URI=on-11-2-11>.
- [14] B. J. Frey. *Graphical Models for Machine Learning and Digital Communication*. Adaptive Computation and Machine Learning. The MIT Press, 1998. ISBN 026206202X; 9780262062022.
- [15] C. Gini. *Variabilità e mutabilità: contributo allo studio delle distribuzioni e delle relazioni statistiche.[Fasc. I.]*. Tipogr. di P. Cuppini, 1912.
- [16] L. Gu, J. Huang, and L. Yang. On the representational power of restricted boltzmann machines for symmetric functions and boolean functions. *IEEE Transactions on Neural Networks and Learning Systems*, 30(5):1335–1347, 2019. doi: 10.1109/TNNLS.2018.2868809.
- [17] W. K. Hastings. Monte Carlo sampling methods using Markov chains and their applications. *Biometrika*, 57(1):97–109, 04 1970. ISSN 0006-3444. doi: 10.1093/biomet/57.1.97. URL <https://doi.org/10.1093/biomet/57.1.97>.

- [18] M. Hibat-Allah, M. Ganahl, L. E. Hayward, R. G. Melko, and J. Carrasquilla. Recurrent neural network wave functions. *Phys. Rev. Research*, 2:023358, Jun 2020. doi: 10.1103/PhysRevResearch.2.023358. URL <https://link.aps.org/doi/10.1103/PhysRevResearch.2.023358>.
- [19] A. Kandala, A. Mezzacapo, K. Temme, M. Takita, M. Brink, J. M. Chow, and J. M. Gambetta. Hardware-efficient variational quantum eigensolver for small molecules and quantum magnets. *Nature*, 549(7671):242–246, 2017. doi: 10.1038/nature23879. URL <https://doi.org/10.1038/nature23879>.
- [20] A. Y. Kitaev, A. Shen, M. N. Vyalyi, and M. N. Vyalyi. *Classical and quantum computation*. American Mathematical Soc., 2002.
- [21] I. Loshchilov and F. Hutter. Decoupled weight decay regularization, 2017. URL <https://arxiv.org/abs/1711.05101>.
- [22] J. R. McClean, J. A. Parkhill, and A. Aspuru-Guzik. Feynman’s clock, a new variational principle, and parallel-in-time quantum dynamics. *Proceedings of the National Academy of Sciences*, 110(41):E3901–E3909, 2013. doi: 10.1073/pnas.1308069110. URL <https://www.pnas.org/doi/abs/10.1073/pnas.1308069110>.
- [23] J. R. McClean, S. Boixo, V. N. Smelyanskiy, R. Babbush, and H. Neven. Barren plateaus in quantum neural network training landscapes. *Nature Communications*, 9(1):4812, 2018. doi: 10.1038/s41467-018-07090-4. URL <https://doi.org/10.1038/s41467-018-07090-4>.
- [24] G. F. Montufar, J. Rauh, and N. Ay. Expressive power and approximation errors of restricted boltzmann machines. In J. Shawe-Taylor, R. Zemel, P. Bartlett, F. Pereira, and K. Weinberger, editors, *Advances in Neural Information Processing Systems*, volume 24. Curran Associates, Inc., 2011. URL <https://proceedings.neurips.cc/paper/2011/file/8e98d81f8217304975ccb23337bb5761-Paper.pdf>.
- [25] M. Schuld, R. Sweke, and J. J. Meyer. Effect of data encoding on the expressive power of variational quantum-machine-learning models. *Phys. Rev. A*, 103:032430, Mar 2021. doi: 10.1103/PhysRevA.103.032430. URL <https://link.aps.org/doi/10.1103/PhysRevA.103.032430>.
- [26] O. Sharir, A. Shashua, and G. Carleo. Neural tensor contractions and the expressive power of deep neural quantum states, 2021. URL <https://arxiv.org/abs/2103.10293>.
- [27] S. Sorella, M. Casula, and D. Rocca. Weak binding between two aromatic rings: Feeling the van der waals attraction by quantum monte carlo methods. *The Journal of Chemical Physics*, 127(1):014105, 2007. doi: 10.1063/1.2746035. URL <https://doi.org/10.1063/1.2746035>.
- [28] X.-Q. Sun, T. Nebabu, X. Han, M. O. Flynn, and X.-L. Qi. Entanglement features of random neural network quantum states, 2022. URL <https://arxiv.org/abs/2203.00020>.

- [29] G. Torlai, G. Mazzola, J. Carrasquilla, M. Troyer, R. Melko, and G. Carleo. Neural-network quantum state tomography. *Nature Physics*, 14(5):447–450, 2018. doi: 10.1038/s41567-018-0048-5. URL <https://doi.org/10.1038/s41567-018-0048-5>.
- [30] V. Vargas-Calderón, H. Vinck-Posada, and F. A. González. Phase diagram reconstruction of the bose–hubbard model with a restricted boltzmann machine wavefunction. *Journal of the Physical Society of Japan*, 89(9):094002, 2020.
- [31] F. Vicentini, D. Hofmann, A. Szabó, D. Wu, C. Roth, C. Giuliani, G. Pescia, J. Nys, V. Vargas-Calderon, N. Astrakhantsev, and G. Carleo. Netket 3: Machine learning toolbox for many-body quantum systems, 2021. URL <https://arxiv.org/abs/2112.10526>.
- [32] D. R. Vivas, J. Madroñero, V. Bucheli, L. O. Gómez, and J. H. Reina. Neural-network quantum states: A systematic review, 2022. URL <https://arxiv.org/abs/2204.12966>.
- [33] L. G. Wright and P. L. McMahon. The capacity of quantum neural networks. In *Conference on Lasers and Electro-Optics*, page JM4G.5. Optica Publishing Group, 2020. URL http://opg.optica.org/abstract.cfm?URI=CLEO_QELS-2020-JM4G.5.
- [34] D. Wu, L. Wang, and P. Zhang. Solving statistical mechanics using variational autoregressive networks. *Phys. Rev. Lett.*, 122:080602, Feb 2019. doi: 10.1103/PhysRevLett.122.080602. URL <https://link.aps.org/doi/10.1103/PhysRevLett.122.080602>.
- [35] D. Wu, R. Rossi, and G. Carleo. Unbiased monte carlo cluster updates with autoregressive neural networks. *Phys. Rev. Research*, 3:L042024, Nov 2021. doi: 10.1103/PhysRevResearch.3.L042024. URL <https://link.aps.org/doi/10.1103/PhysRevResearch.3.L042024>.
- [36] L. Xiao, J. Pennington, and S. Schoenholz. Disentangling trainability and generalization in deep neural networks. In H. D. III and A. Singh, editors, *Proceedings of the 37th International Conference on Machine Learning*, volume 119 of *Proceedings of Machine Learning Research*, pages 10462–10472. PMLR, 13–18 Jul 2020.
- [37] T. Zhao, S. De, B. Chen, J. Stokes, and S. Veerapaneni. Overcoming barriers to scalability in variational quantum monte carlo. In *Proceedings of the International Conference for High Performance Computing, Networking, Storage and Analysis, SC ’21*, New York, NY, USA, 2021. Association for Computing Machinery. ISBN 9781450384421. doi: 10.1145/3458817.3476219. URL <https://doi.org/10.1145/3458817.3476219>.

Appendix A. Optimisation of neural quantum states

Both VMC and NQS training have hyper-parameters that dictate the behaviour of the variational energy optimisation. Since the aim of this study is to train NQSSs in the

VMC setup with the greatest possible quality, we adopt a fruitful machine learning strategy that targets the best set of hyper-parameters, namely hyper-parameter tuning. Hyper-parameter tuning is a difficult meta-optimisation task that, in our case, thrives to answer the questions: what does the training algorithm look like, and what is neural quantum state architecture that produce the lowest variational energy?

Let us start by stating the hyper-parameters for VMC. The two main components of VMC are the sampler and the optimiser. The sampler dictates how the sample \mathcal{M} of eq. (5) is built, and the optimiser is a rule for updating the parameters θ of the NQS.

In the NQS literature, it is common to find that stochastic reconfiguration (SR) [27] is used in combination with stochastic gradient descent (SGD) as an optimiser. SR takes into account the geometry of the variational energy landscape to update parameters in the directions that yield maximum descent. However, we experimented on optimisation instances that used the RBM NQS (eq. (6)) with different numbers of hidden neurons using both SR+SGD and AdamW [21] and found no significant difference in performance. On the contrary, AdamW was faster, which is why we chose it as the optimisation method for all of the experiments shown in the main text. We consider its learning rate as the sole hyper-parameter of the optimiser. Regarding the sampler, we consider the number of parallel Markov chains and the number of total samples as its two hyper-parameters. In the case of an autoregressive NQS, no Markov chains are considered, and the sampler only has the number of total samples hyper-parameter.

The hyper-parameters for the architecture of the NQs are different for the RBM and the autoregressive ansätze. For the RBM, the hyper-parameter is $\alpha := N_H/(N_S + N_T)$, which specifies the proportion of hidden neurons with respect to the visible neurons of the RBM. For the autoregressive ansatz, the autoregressive neural network η in eq. (7) has two hyper-parameters: the number of layers N_L , and the number of hidden neurons N_H of each layer, with the property that the layers are masked in such a way that the conditional probability of a spin taking a value depends only on the values of the previous spins.

The hyper-parameter tuning algorithm that we used is the tree-structured Parzen estimator [9] provided in the Optuna package [2]. TSPE works by updating the priors with Gaussian mixture models: one for the hyper-parameters x with lowest loss $\ell(x)$, and one for the ones with highest loss $g(x)$. Then, at each new hyper-parameter trial, TSPE recommends a new set of hyper-parameters x^* that maximises $l(x^*)$ with respect to $g(x^*)$. The priors for each hyper-parameter are shown in table A1. Hyper-parameter tuning was conducted for 100 different hyper-parameter sets for each ansatz, and for each combination of number of physical spins N_S and number of time spins N_T .

Appendix A.1. Turning on the clock adiabatically

We adopt the strategy by Barison et al. [6] of turning on the clock gradually. This means that we perform the energy (or infidelity) minimisation of eq. (2) for a total

Table A1. Prior distribution of hyper-parameters for the tree-structured Parzen estimator.

NQS	Hyper-parameter	Support	Prior
RBM & AR	Number of samples	$[256, 2048]$	Uniform
	Learning rate	$[10^{-4}, 1]$	Loguniform
RBM	Number of Markov chains	$\{4, 8, 16\}$	Uniform
	α	$\{1, \dots, 5\}$	Uniform
AR	N_L	$\{1, 2, 3\}$	Uniform
	N_H	$\{2, 4, 8, 16, 32\}$	Uniform

time $T_k = kT/20$, starting from $k = 1$ and ending at $k = 20$. This strategy simplifies learning overall, as it gradually increases the learning problem difficulty: for small k , the evolution is for small times, meaning that the state of the physical system remains almost unchanged throughout evolution. As k gets larger, the state of the physical system starts to significantly change between consecutive time steps.